

Standing Between Past and Future: Spatio-Temporal Modeling for Multi-Camera 3D Multi-Object Tracking

Ziqi Pang¹, Jie Li², Pavel Tokmakov², Dian Chen², Sergey Zagoruyko³, Yu-Xiong Wang¹
 University of Illinois Urbana-Champaign¹, Toyota Research Institute², Woven Planet Level-5³

{zqip2, yxw}@illinois.edu

Abstract

This work proposes an end-to-end multi-camera 3D multi-object tracking (MOT) framework. It emphasizes spatio-temporal continuity and integrates both past and future reasoning for tracked objects. Thus, we name it “Past-and-Future reasoning for Tracking” (PF-Track). Specifically, our method adapts the “tracking by attention” framework and represents tracked instances coherently over time with object queries. To explicitly use historical cues, our “Past Reasoning” module learns to refine the tracks and enhance the object features by cross-attending to queries from previous frames and other objects. The “Future Reasoning” module digests historical information and predicts robust future trajectories. In the case of long-term occlusions, our method maintains the object positions and enables re-association by integrating motion predictions. On the nuScenes dataset, our method improves AMOTA by a large margin and remarkably reduces ID-Switches by 90% compared to prior approaches, which is an order of magnitude less. The code and models are made available at <https://github.com/TRI-ML/PF-Track>.

1. Introduction

Reasoning about object trajectories in 3D is the cornerstone of autonomous navigation. While many LiDAR-based approaches exist [42, 65, 70], their applicability is limited by the cost and reliability of the sensor. Detecting, tracking, and forecasting object trajectories only with cameras is hence a critical problem. Significant progress has been achieved on these tasks separately, but they have been historically primarily studied in isolation and combined into a full-stack pipeline in an ad-hoc fashion.

In particular, 3D detection has attracted a lot of attention [21, 27, 28, 32, 60], but associating these detections over time has been mostly done independently from localization [20, 37, 49]. Recently, a few approaches for end-to-end detection and tracking have been proposed, but they

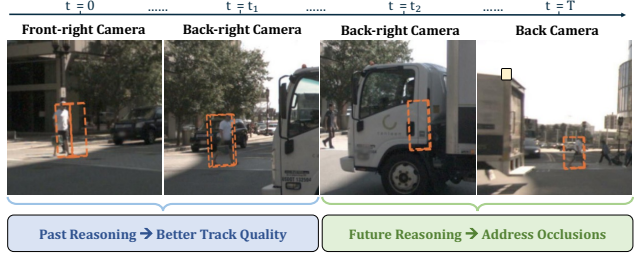


Figure 1. We visualize the output of our model by projecting predicted 3D bounding boxes onto images. In the beginning, image-based detection can be inaccurate ($t = 0$) due to depth ambiguity. With “Past Reasoning”, the bounding box quality ($t = t_1$) gradually improves by leveraging historical information. With “Future Reasoning”, our PF-Track predicts the long-term motions of objects and maintains their states even under occlusions ($t = t_2$). This enables re-association without explicit re-identification ($t = T$), as the object ID does not switch. Our PF-Track further combines past and future reasoning in a joint framework to improve spatio-temporal coherence.

operate on neighboring frames and fail to integrate longer-term spatio-temporal cues [6, 13, 39, 72]. In the prediction literature, on the other hand, it is common to assume the availability of ground truth object trajectories and HD maps [3, 7, 12, 66]. A few attempts for a more realistic evaluation have been made [17, 22], focusing only on the prediction performance.

In this paper, we argue that multi-object tracking can be dramatically improved by jointly optimizing the detection-tracking-prediction pipeline, especially in a camera-based system. We provide an intuitive example from our real-world experiment in Fig. 1. At first, the pedestrian is fully visible, but a model with only single-frame information makes a prediction with large deviation (frame $t = 0$ in Fig. 1). After this, integrating the temporal information from the past gradually corrects the error over time (frame $t = t_1$ in Fig. 1), by capitalizing on the notion of spatio-temporal continuity. Moreover, as the pedestrian becomes fully occluded (frame $t = t_2$ in Fig. 1), we can still pre-

dict their location by using the aggregated past information to estimate a future trajectory. Finally, we can successfully track the pedestrian on re-appearance via long-term prediction, resulting in correct re-association (frame $t = T$ in Fig. 1). The above robust spatio-temporal reasoning is enabled by seamless, bi-directional integration of past and future information, which starkly contrasts with the mainstream pipelines for vision-based, multi-camera, 3D MOT.

To this end, we propose an end-to-end framework for joint 3D object detection, tracking, and trajectory prediction for the task of 3D MOT, as shown in Fig. 2, adopting the “tracking by attention” [40, 71, 72] paradigm. Compared to our closest baseline under the same paradigm [72], we are different in explicit past and future reasoning: a 3D object query consistently represents the object over time, propagates the spatio-temporal information of the object across frames, and generates the corresponding bounding boxes and future trajectories. To exploit spatio-temporal cues, our algorithm leverages simple attention operations to capture object dynamics and interactions, which are then used for track refinement and robust, long-term trajectory prediction. Finally, we close the loop by integrating predicted trajectories back into the tracking module to replace missing detections (*e.g.*, due to an occlusion). To highlight the capability of joint past and future reasoning, our method is named “Past-and-Future reasoning for Tracking” (PF-Track).

We provide a comprehensive evaluation of PF-Track on nuScenes [3] and demonstrate that joint modeling of past and future information provides clear benefits for object tracking. In particular, PF-Track decreases ID-Switches by over 90% compared to previous multi-camera 3D MOT methods.

To summarize, our contributions are as follows.

1. We propose an end-to-end vision-only 3D MOT framework that utilizes object-level spatio-temporal reasoning for both past and future information.
2. Our framework improves the quality of tracks by cross-attending to features from the “**past**”.
3. We propose a joint tracking and prediction pipeline, whose constituent part is “Future Reasoning”, and demonstrate that tracking can explicitly benefit from long-term prediction into the “**future**”.
4. Our method establishes new state-of-the-art on large-scale nuScenes dataset [3] with significant improvement for both AMOTA and ID-Switch.

2. Related Work

LiDAR-Based 3D MOT. The majority of prior works in 3D MOT leverage the LiDAR modality. Due to the recent advances in LiDAR-based 3D detection [25, 68], especially the reliable range information, most state-of-the-art 3D MOT algorithms adopt a “tracking-by-detection”

paradigm [63]. Given single frame detection outputs, different approaches have been proposed to improve data association [42, 65, 70], motion propagation [9, 75], and life cycling [42, 58]. However, most of these works assume the location accuracy of each detection output. Therefore, data association is usually conducted based on location, optionally combined with abstracted object attributes (*e.g.*, 3D IoU [63], 3D GIoU [42], and L2 [68]). This bias causes the proposed systems to be fragile when migrated into the camera modality, where 3D detection suffers from higher localization uncertainty. Although the latest methods incorporate learning-based algorithms to improve association with high-fidelity features such as low-level features from point cloud [52] or intermediate features from cameras [9], these approaches are built on top of the LiDAR-based frameworks and share their dependence on localization quality.

Camera-based 2D MOT. Camera-based multi-object tracking in 2D is a classic task in computer vision. Dominated by “tracking by detection” paradigm [2], 2D MOT has seen more success in leveraging high-fidelity features [44, 55, 67, 73]. Earlier works like DeepSORT [67] leveraged intermediate features from a deep net to measure appearance similarity. FairMOT [73] employed an additional Re-ID branch to learn discriminative features in a detection network. TransMOT [44] proposed to incorporate spatio-temporal features using a graph network.

Camera-based 3D MOT. Camera-based 3D MOT has recently drawn more attention in autonomous driving applications thanks to advances in monocular depth estimation [14, 16, 18] and image-based 3D object detection [21, 27, 28, 32, 33, 43, 47, 59, 60]. Early methods adapted the 2D MOT algorithms and lifted the 2D tracking result using monocular depth [56, 75]. More recent approaches employ additional 3D information in data association [20, 37, 49]. Luiten et al. [37] proposed to leverage 3D reconstruction, and Hu et al. [20] augmented the 2D Re-ID features with 3D attributes (*e.g.* depth and orientation). CC-3DT [13] merges the multi-view camera features for identical objects within a single timestamp to improve the cross-time cross-view association. However, considering or correcting the high uncertainty and bias in camera-based 3D detection has been less explored. In this work, we leverage long-term object reasoning, especially past reasoning, to improve the quality of 3D bounding boxes.

Tracking by Attention. A rising trend in MOT is the “tracking by attention” paradigm [40, 53, 71, 72] inspired by the novel transformer-based detection architecture DETR [4]. MOTR [71] and Trackformer [40] extended the query-based detection framework in DETR [4] by propagating queries across different frames. In this paradigm, the data association is replaced by “detection” in the cur-

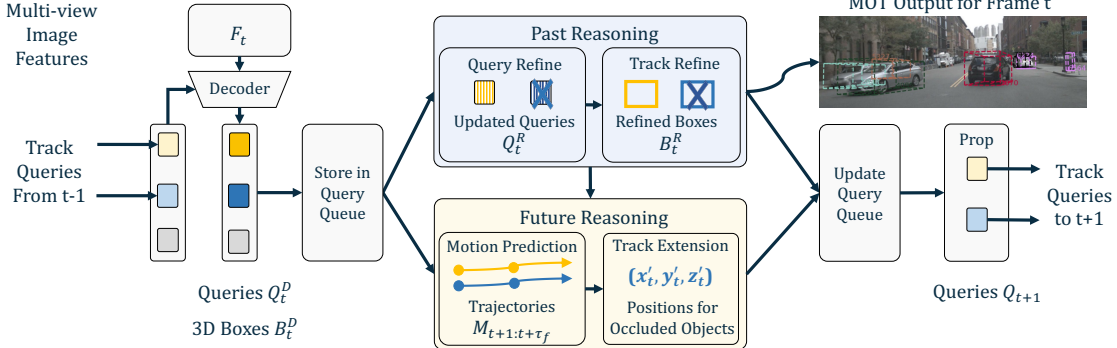


Figure 2. **PF-Track Framework.** (Best viewed in color, details in Sec. 3.1) PF-Track represents objects as queries, decodes image features, and predicts bounding boxes. To improve spatio-temporal coherence, we incorporate novel “Past Reasoning” and “Future Reasoning” modules. (1) “Past Reasoning” refines the features of queries and bounding boxes of tracks by exploiting the historical information in the query queue. (2) “Future Reasoning” improves the propagation of queries across frames by estimating long-term future trajectories. Furthermore, if an object is lost due to low confidence or occlusion (blue squares with \times), the “track extension” module can use a long-term trajectory to maintain its location. Eventually, PF-Track incorporates past and future reasoning jointly for 3D MOT.

rent frame with a set of track queries. MUTR3D [72] proposed the first framework applying this paradigm to the 3D MOT domain. It uses a 3D track query to jointly model object features across timestamps and multi-views. Despite its improvement at the time, MUTR3D mostly follows the designs of 2D MOT methods and does not include special treatment to improve the localization quality of tracks and better propagate the queries to future frames. Our proposed algorithm also operates in the “tracking by attention” paradigm but extends the temporal horizon of existing methods. In particular, we demonstrate that joint past and future reasoning can improve the tracking framework by providing a strong spatio-temporal object representation.

Motion Prediction. Predicting agent trajectories is critical for self-driving [15, 23, 34, 41, 48, 51, 69]. The most common setting is to predict from clean tracks annotated by humans or auto-labeling [7, 12, 54, 66]. Numerous studies focus on end-to-end prediction from perception [5, 19, 29, 38, 45, 46, 50, 61, 62, 64, 74], especially how to improve motion prediction directly from perception. However, our objective is different: Could a motion prediction model benefit 3D MOT? In the 2D setting, this problem has received only limited attention recently [11]. Our algorithm advances this research into a more challenging multi-camera, 3D scenario and does not require explicit re-identification.

3. Method: PF-Track

This section introduces our novel 3D multi-object tracking framework, shown in Fig. 2. It is centered around explicit past and future modeling of object trajectories in an end-to-end framework. We first provide an overview of the pipeline in Sec. 3.1, and then explain how to efficiently leverage “Past” (Sec. 3.2) and “Future” (Sec. 3.3) informa-

tion. Finally, we summarize the losses used in our framework in Sec. 3.4.

3.1. PF-Track Pipeline

Our proposed PF-Track iteratively uses a set of object queries [40, 71, 72] to tackle multi-view, multi-object, 3D tracking. At each timestamp t , given K images \mathbf{I}_t^k from surrounding cameras, the objective of 3D MOT is to generate object detections with consistent IDs across frames, denoted by $\mathbf{B}_t = \{\mathbf{b}_t^i\}$, where i is an object ID.

The first step in our framework is to receive the object queries propagated from the previous frame (yellow and blue squares in Fig. 2), which represents the tracked objects:

$$\mathbf{Q}_t \leftarrow \text{Prop}(\mathbf{Q}_{t-1}). \quad (1)$$

Such a query-based design naturally addresses the task of tracking as the queries carry the identity of objects over time. Apart from queries from the previous frame that represent tracked instances, we also add a fixed number of detection queries (gray squares in Fig. 2) to discover new objects. In practice, we use 500 detection queries initialized as learnable embeddings.

To predict 3D bounding boxes and update queries with the latest image inputs, PF-Track adopts an attention-based detection architecture [4, 76] to decode image features \mathbf{F}_t with object queries $\mathbf{Q}_t = \{\mathbf{q}_t^i\}$:

$$\mathbf{B}_t^D, \mathbf{Q}_t^D \leftarrow \text{Decoder}(\mathbf{F}_t, \mathbf{Q}_t), \quad (2)$$

\mathbf{B}_t^D and \mathbf{Q}_t^D are the detected 3D bounding boxes and updated query features, respectively. After they receive the current frame information, both \mathbf{B}_t^D and \mathbf{Q}_t^D are subjected to past and future reasoning before becoming the boxes for

output and queries for the next frame. In the decoding process, while the design of PF-Track is agnostic to query-based detection algorithms, we mainly adopt a current state-of-the-art 3D detector, PETR [32], for experiments.

3D Object Queries. A constituent part of the above process is the set of object queries. Each of them represents a unique 3D object with a feature vector \mathbf{f}_t^i and a 3D location \mathbf{c}_t^i : $\mathbf{q}_t^i = \{\mathbf{f}_t^i, \mathbf{c}_t^i\}$. Here we highlight that the query position is an active participant in the decoding process of Eqn. 2, where the decoder lifts the 3D positions into positional embeddings to concentrate on the image regions relevant to the spatial locations of the object.

Past and Future Reasoning for Refinement and Propagation. After decoding the queries and boxes from single-frame image features, PF-Track conducts past and future reasoning to (1) refine the current detections and queries; (2) propagate the queries to the next timestamp, as in Fig. 2.

“Past Reasoning” $\mathbf{PR}(\cdot)$ aggregates the information from previous frames to generate refined query features and bounding boxes:

$$\mathbf{Q}_t^R, \mathbf{B}_t^R \leftarrow \mathbf{PR}(\mathbf{Q}_t^D, \mathbf{B}_t^D, \mathbf{Q}_{t-\tau_h:t-1},). \quad (3)$$

In practice, the historical queries $\mathbf{Q}_{t-\tau_h:t-1}$ come from a **query queue** that maintains the queries from past τ_h frames (h for “history”). After processing them, past reasoning outputs refined queries and detections, denoted as \mathbf{Q}_t^R and \mathbf{B}_t^R , respectively (R is short for “refined”).

After past reasoning, the “Future Reasoning” module $\mathbf{FR}(\cdot)$ improves the coherence of object positions from the aspect of query propagation. It achieves this by forecasting the motions up to τ_f frames (f for “future”) and transforms the positions of queries accordingly:

$$\mathbf{Q}_{t+1}, \mathbf{M}_{t+1:t+\tau_f} \leftarrow \mathbf{FR}(\mathbf{Q}_t^R, \mathbf{Q}_{t-\tau_h:t-1}). \quad (4)$$

Specifically, future reasoning extracts the object dynamics from historical query features to predict the trajectories $\mathbf{M}_{t+1:t+\tau_f}$. The single-step movement \mathbf{M}_{t+1} is leveraged to propagate the current queries \mathbf{Q}_t^R to the next timestamp, and long-term trajectories $\mathbf{M}_{t+1:t+\tau_f}$ are used for addressing occlusions. The “Track Extension” in Fig. 2 refers to occlusion reasoning through the predicted trajectories.

PF-Track iteratively executes the above procedures. The refined 3D bounding boxes \mathbf{B}_t^R are the output for 3D MOT.

3.2. Past Reasoning

To address the uncertainty of detection in vision-only 3D localization, past reasoning focuses on two aspects: (1) enhancing the query features by attending to historical embeddings; (2) refining the tracks by adjusting the bounding boxes using the improved query features.

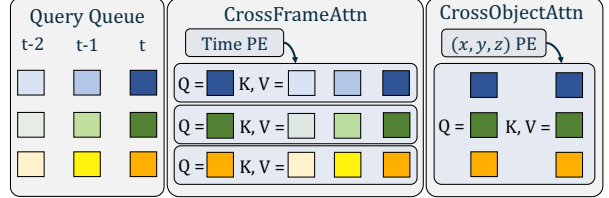


Figure 3. **Query Refinement.** (Best viewed in color.) “Cross-frame” and “Cross-object” attention modules process the query queue to capture the temporal and inter-object relationship, respectively. They apply the positional encoding for time t and spatial locations (x, y, z) , respectively.

Query Refinement: from \mathbf{Q}_t^D to \mathbf{Q}_t^R . We first apply attention across the time and instance axes to explicitly update the query features with historical information, as illustrated in Fig. 3. “Cross-frame” attention encourages the interplay of features within a history window of τ_h frames per object:

$$\begin{aligned} \mathbf{f}_t^i &\leftarrow \mathbf{CrossFrameAttn}(\mathbf{Q} = \mathbf{f}_t^i, \\ &\quad \mathbf{K} = \mathbf{f}_{t-\tau_h:t}^i, \mathbf{V} = \mathbf{f}_{t-\tau_h:t}^i, \quad (5) \\ &\quad \mathbf{PE} = \mathbf{Pos}(t - \tau_h : t)), \end{aligned}$$

where, $\mathbf{Pos}(t - \tau_h : t)$ converts the timestamps into positional embedding, and the history frames with empty features are ignored for attention computation.

Then past reasoning applies “Cross-object” attention to incorporate the context information and encourage more discriminative feature representation for each object. In particular, cross-object attention (Fig. 3, right) further updates the query features via

$$\begin{aligned} \mathbf{f}_t^{1:N_t} &\leftarrow \mathbf{CrossObjectAttn}(\mathbf{Q}, \mathbf{K}, \mathbf{V} = \mathbf{f}_t^{1:N_t}, \quad (6) \\ &\quad \mathbf{PE} = \mathbf{Pos}(\mathbf{c}^{1:N_t})), \end{aligned}$$

where cross-object attention exchanges the features of N_t objects guided by their 3D positional embedding $\mathbf{Pos}(\mathbf{c}^{1:N_t})$. The final output $\mathbf{f}_t^{1:N_t}$ eventually becomes the refined feature vectors in queries \mathbf{Q}_t^R .

As a brief remark, decoupling cross-frame and cross-object attention exhibit two advantages. Firstly, separating attention across frames (cross-frame) and objects (cross-object) enable us to design specialized positional encoding of time and locations for each of them. Secondly, it decreases the computational complexity from the $\mathcal{O}(N_t^2\tau_h^2)$ for the global cross-attention to $\mathcal{O}(N_t^2 + N_t\tau_b^2)$, which is significantly smaller. Our design is also closely related to how motion prediction methods [15, 41] model spatial-temporal relationship.

Track Refinement: from \mathbf{B}_t^D to \mathbf{B}_t^R . With the queries refined by historical information, past reasoning further uses track refinement to improve the 3D bounding box quality. As specified in Eqn. 7, we apply an MLP to predict

the updated properties of objects, including center residuals ($\Delta x, \Delta y, \Delta z$), size (l, w, h), orientations (θ), velocities (\mathbf{v}), and scores (s):

$$(\Delta x, \Delta y, \Delta z, l, w, h, \theta, \mathbf{v}, s)^i = \text{MLP}(\mathbf{f}_t^i). \quad (7)$$

These are then used to adjust the original boxes as follows:

$$\mathbf{b}_t^i = (\Delta x + x_t^i, \Delta y + y_t^i, \Delta z + z_t^i, l, w, h, \theta, \mathbf{v}, s), \quad (8)$$

resulting in \mathbf{B}_t^R , which is the final model output at frame t

3.3. Future Reasoning

“Future Reasoning” concentrates on improving the propagation of queries across frames to benefit spatio-temporal coherence. It first learns a trajectory prediction, which is used for moving queries across adjacent frames. Then future reasoning exploits the predicted long-term trajectories for maintaining the positions of occluded or noisy tracks.

Motion Prediction. Trajectory prediction supervises the model’s ability to capture object movements and is further beneficial for propagating query positions across timestamps. Similar to past reasoning, our future reasoning model adopts a simple attention-based architecture. Firstly, we generate the embeddings for τ_f timestamps $\mathbf{f}_{t+1:t+\tau_f}^i$ with a cross frame attention:

$$\begin{aligned} \text{CrossFrameAttn}(\mathbf{Q} = \mathbf{f}_{t+1:t+\tau_f}^i, \\ \mathbf{K} = \mathbf{f}_{t-\tau_h:t}^i, \mathbf{f}_{t-\tau_h:t}^i, \\ \mathbf{PE} = \mathbf{Pos}(t - \tau_h : t + \tau_f)), \end{aligned} \quad (9)$$

where $\mathbf{f}_{t+1:t+\tau_f}^i$ are initialized as zeros, and historical feature $\mathbf{f}_{t-\tau_h:t}^i$ serves as the source of information. Then the movement at every timestamp is decoded by an MLP:

$$\mathbf{m}_{t+1:t+\tau_f}^i = \text{MLP}(\mathbf{f}_{t+1:T+\tau_f}^i), \quad (10)$$

and the object trajectory in the 3D space can be recovered by combining these frame-level outputs. Our architecture is inspired by SceneTransformer [41], which also employs a fully-attention-based architecture.

The predicted trajectories $\mathbf{m}_{t+1:t+\tau_f}^i$ have better fidelity compared to the velocities \mathbf{v} predicted by the decoder in \mathbf{B}_t^R and \mathbf{B}_t^D . Thus, we can propagate the positions of queries by adding a single step of the trajectory:

$$\mathbf{c}_{t+1}^i = \mathbf{c}_t^i + \mathbf{m}_{t:t+1}^i. \quad (11)$$

Track Extension. To handle occlusions or noisy observations, we propose to extend the tracks using the predicted trajectories. In particular, we replace missing or low-confidence detections with the output of our motion prediction module, which is initialized from confident observations. Previous 3D MOT approaches either terminate the

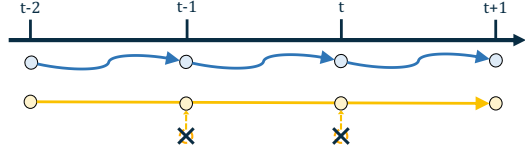


Figure 4. **Track extension.** PF-Track updates object positions and predicts future trajectories at every timestamp (top row). However, if the object cannot be confidently localized (e.g. due to occlusion or a noisy observation, bottom row at frames $t - 1$ and t), our method will rely on the long-term trajectories predicted from confident timestamps (frame $t - 2$) to infer the positions of this object and ignore the noisy observations (crossed-out circles).

tracks or prolong them with heuristic motion models (e.g. Kalman filters) under such conditions. However, these solutions both could lead to ID-Switches due to “early termination” [42] or false associations. In contrast, our learnable motion prediction module and track extension strategy can be more accurate and robust.

We visualize the high-level intuition in Fig. 4 and provide more details in the appendix (Sec. B.2). In Fig. 4, the long-term trajectories assist the propagation of the yellow instance (bottom row). When PF-Track encounters noisy observation or occlusion cases, it relies on the motion predictions from previous confident frames to simulate the movements of occluded objects. In extreme cases, our model is able to handle occlusion length of $\tau_f - 1$ frames. Our ablation study in Sec. 4.4 demonstrates that track extension can decrease ID-Switch by a large margin. To the best of our knowledge, we are the first to incorporate long-term prediction into a query-based framework and address occlusion without explicit re-identification.

3.4. Loss Functions

Our final loss function is defined as follows:

$$\begin{aligned} \mathcal{L} = & \lambda_{cls}^D \mathcal{L}_{cls}^D + \lambda_{box}^D \mathcal{L}_{box}^D + \\ & \lambda_{cls}^R \mathcal{L}_{cls}^R + \lambda_{box}^R \mathcal{L}_{box}^R + \lambda_f \mathcal{L}_f \end{aligned} \quad (12)$$

where \mathcal{L}_{cls} and \mathcal{L}_{cls}^R are focal loss [31] with the coefficients of λ_{cls}^D and λ_{cls}^R . They supervise the classification scores of \mathbf{B}_t^D and \mathbf{B}_t^R (as in Fig. 2). \mathcal{L}_{box}^D and \mathcal{L}_{box}^R are both L1 loss applied to \mathbf{B}_t^D and \mathbf{B}_t^R for bounding box regression. Their coefficients are λ_{box}^D and λ_{box}^R . The motion prediction loss \mathcal{L}_f is an L1 loss between the movements of predicted and ground-truth trajectories, weighted by λ_f . The ground-truth assignment couples a query with a consistent ground-truth instance over time to encourage ID consistency. We discuss more details in the appendix (Sec. B.1).

	AMOTA ↑	AMOTP ↓	RECALL ↑	MOTA ↑	IDS ↓
<i>Validation Split</i>					
DEFT [6]	0.201	N/A	N/A	0.171	N/A
QD3DT [20]	0.242	1.518	39.9%	0.218	5646
MUTR3D [72]	0.294	1.498	42.7%	0.267	3822
TripletTrack [39]	0.285	1.485	N/A	N/A	N/A
CC-3DT* [13]	0.429	1.257	53.4%	0.385	2219
PF-Track-S (Ours)	0.408	1.343	50.7%	0.376	166
PF-Track-F (Ours)	0.479	1.227	59.0%	0.435	181
<i>Test Split</i>					
CenterTrack [75]	0.046	1.543	23.3%	0.043	3807
PermaTrack [56]	0.066	1.491	18.9%	0.060	3598
DEFT [6]	0.177	1.564	33.8%	0.156	6901
QD3DT [20]	0.217	1.550	37.5%	0.198	6856
MUTR3D [72]	0.270	1.494	41.1%	0.245	6018
TripletTrack [39]	0.268	1.504	40.0%	0.245	1144
CC-3DT* [13]	0.410	1.274	53.8%	0.357	3334
PF-Track-F (Ours)	0.434	1.252	53.8%	0.378	249

Table 1. Comparison with state-of-the-art camera-based 3D MOT algorithms on nuScenes [3]. “S” and “F” denotes our model trained with small and full resolution settings (clarified in Sec. 4.2). Our approach has a significant advantage on both AMOTA and ID-Switch, where ID-Switch is almost 90% less and *an order of magnitude smaller* compared to other methods. (*) indicates concurrent works.

4. Experiments

4.1. Datasets and Metrics

Datasets. We conduct experiments on the large-scale self-driving dataset nuScenes [3]. It contains 1,000 video sequences with multiple modalities, including RGB images from 6 surrounding cameras, and point clouds from LiDAR and Radar. In this paper, we use camera sensors only. Every sequence spans roughly 20 seconds with keyframes annotated at 2Hz. The dataset provides 1.4M 3D bounding boxes covering 10 types of common objects on the road. For the tracking task, nuScenes selects a subset of 7 mobile categories, such as cars, pedestrians, and motorcycles, and excludes static objects like traffic cones.

Metrics. We strictly follow the official evaluation metrics for multi-object tracking tasks from nuScenes. It modifies CLEAR MOT metrics [1] by considering multiple recall thresholds. The main metric is “Average Multiple-Object Tracking Accuracy” (AMOTA) [63]. Meanwhile, we also consider other analytical metrics such as “Identity Switches” (IDS) and AMOTP.

4.2. Implementation Details

Due to space limits, we clarify two training settings here and describe more implementation detail in the appendix (Sec. B). In our implementation, every training sample contains three adjacent frames from different timestamps. However, it requires extensive computation as every frame

contains six high-resolution images. Therefore, we adapt two settings that downsample images to different resolutions, motivated by PETR [32].

Full-resolution. On every time frame, we cropped the raw resolution images, 1600×900 to 1600×640 , leaving the sky area out. However, training on this resolution wouldn’t fit in a single A100 GPU. Thus, we first pretrain the backbone with single-frame detection for 24 epochs following some previous works [56]. Then we fix the backbone and train the tracker on three-frame samples for another 24 epochs. We only use this setting for full model results indicated with “-F” in Tab. 1.

Small-resolution. We apply a small-resolution setting for all of our ablation analyses unless specified. In this setting, we downsample the cropped images to a resolution of 800×320 . We first train a single-frame detection model for 12 epochs and the tracker on three-frame samples for another 12 epochs.

4.3. State-of-the-art Comparison on nuScenes

In Tab. 1, we compare our model performance with the other published camera-based 3D MOT algorithms on nuScenes [3]. Our approach establishes a new state-of-the-art with significant improvements on every metric. Our AMOTA improves more than 7% on the test set and 12% on the validation set over the previous methods, including a very strong concurrent work [13]. It is worth noting that with more established tracks (higher recall), our ID-Switch number is only 10% of previous methods eliminating more than 90% of the ID-switching errors. This result indicates the strong association ability of our algorithm leveraging both past and future reasoning. The advantage of our model holds even when trained in the low-resolution setting whereas most of the previous works use full-resolution.

4.4. Ablation Studies

Efficacy of Past and Future Reasoning. In Tab. 2, we analyze the importance of individual modules for our model’s performance using the validation set of nuScenes. In particular, we evaluate the following variants. (1) **Baseline**. Our baseline is a tracking-by-attention model without explicit spatio-temporal reasoning (row 1). It is a strong baseline and already outperforms prior work in Tab. 1. (2) **Past Reasoning**. We first analyze the effect of query refinement (row 2), which explicitly incorporates the historical queries via cross-attention. As illustrated, it improves the overall tracking quality. We then further exploit the enhanced feature to refine the 3D bounding boxes of tracks (row 3). It decreases the ID-Switch and AMOTP, which indicates that track refinement is useful for 3D MOT. (3) **Future Reasoning**. Next, we demonstrate that learning to predict object motion and propagate positions (row 4) is beneficial

Index	Past		Future		AMOTA↑	AMOTP↓	IDS↓
	QR	TR	Pred	Ext			
1					0.368	1.421	507
2	✓				0.378	1.414	453
3	✓	✓			0.380	1.408	400
4			✓		0.374	1.402	469
5			✓	✓	0.391	1.360	155
6	✓	✓	✓	✓	0.408	1.343	166

Table 2. **Ablation of PF-Track Modules.** For past reasoning, “QR” and “TR” denote “query refinement” and “track refinement” in Sec. 3.2. For future reasoning, “Pred” and “Ext” denote “motion prediction” and “track extension” in Sec. 3.3. Past and future reasoning improve 3D MOT independently, and PF-Track achieves top results by combining them in an end-to-end framework.

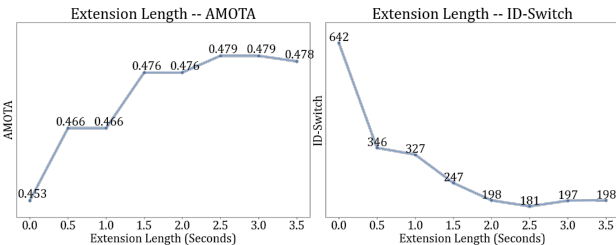


Figure 5. **Track extension assists MOT.** By using the predicted trajectories to maintain the states for low-confidence tracks, we significantly improve AMOTA and decrease ID-Switch.

for modeling object dynamics and leads to improved tracking performance. In addition, using the long-term trajectory predictions to replace low-confidence localizations (row 5) results in a 67% drop in ID-Switches. **(4) Joint Past and Future Reasoning.** Finally, combining past and future reasoning into an end-to-end framework shown in Fig. 2 (row 6), allows our model to achieve top performance. This result confirms that past and future reasoning are mutually beneficial for 3D MOT.

Length of Track Extension. In Fig. 5, we analyze the effect of track extension length on AMOTA and ID-Switches using our best-performing full-resolution model on the validation split of nuScenes. Compared to not using the extension strategy (0.0s), prolonging the tracks strongly improves the performance up to 2 seconds. Then the metrics saturate because only a few objects reappear after such a long period. Please note that these improvements are achieved without explicit re-identification.

Length of Prediction in Future Reasoning. Next, we analyze how the prediction length changes the 3D MOT performance on nuScenes validation split in Tab. 3. Concretely, we train three different full-fledged models with the prediction length of 2.0, 3.0, and 4.0 seconds. The AMOTA and ID-Switch indicate that 4.0s (8 frames) has a slight advantage over 2.0s (4 frames) and 3.0s (6 frames). This result indicates that learning trajectory forecasting with longer hori-

Length	Extention	AMOTA ↑	AMOTP ↓	IDS ↓
2.0s	✗	0.392	1.376	604
2.0s	✓	0.402	1.342	217
3.0s	✗	0.392	1.372	540
3.0s	✓	0.402	1.340	208
4.0s	✗	0.391	1.387	471
4.0s	✓	0.408	1.343	166

Table 3. **Length of motion prediction.** “Extension” means using “track extension”. We train three models with the prediction horizon of 2.0s, 3.0s, and 4.0s. According to AMOTA and IDS, learning a longer prediction benefits tracking.

	AMOTA ↑	AMOTP ↓	IDS ↓
AB3DMOT [63]	0.292	1.333	2419
AB3DMOT [63] ^Ψ	0.329	1.388	2677
CenterPoint [68]	0.233	1.270	2715
CenterPoint [68] ^Ψ	0.383	1.329	3082
SimpleTrack [42]	0.320	1.295	1606
SimpleTrack [42] ^Ψ	0.402	1.324	2053
PF-Track (Ours)	0.408	1.343	166

Table 4. **Comparison with “tracking by detection”.** We apply strong baselines in 3D MOT to PETR [32]: AB3DMOT [63], CenterPoint [68], and SimpleTrack [42]. “Ψ” means that we tune the hyper-parameters of these methods to fit PETR detections, rather than using their original configuration. Our end-to-end approach has significant advantages.

zon benefits our 3D MOT framework.

Comparison with “Tracking by Detection” Baselines.

In Tab. 4, we compare the performance between our end-to-end framework and previous “tracking by detection” algorithms [42, 63, 68], which are strong baselines for LiDAR-based 3D MOT. For these experiments we also use the validation split of nuScenes. For a fair comparison, we evaluate these methods with PETR [32] detections, and tune their hyper-parameters for AMOTA (shown in the table with “Ψ”, details are provided in the appendix, Sec. B.4). The results clearly demonstrate the advantages of our end-to-end approach compared to more traditional, modular frameworks, with improvements being especially a significant on the ID-Switch metric.

Analysis on Prediction from Query Features. While our paper focuses on multi-object tracking, we additionally provide an analysis of prediction performance. We show that predicting end-to-end from object features is advantageous over predicting from low-level object states, such as center positions. Specifically, we train two motion prediction baselines, VectorNet [15] and LSTM [7] using the true-positive tracks from PF-Track following previous studies [38], and report their results in the top rows of Tab. 5. As our method does not use HD-Maps, for a fair comparison, we exclude the parts of motion prediction algorithms that handle HD-

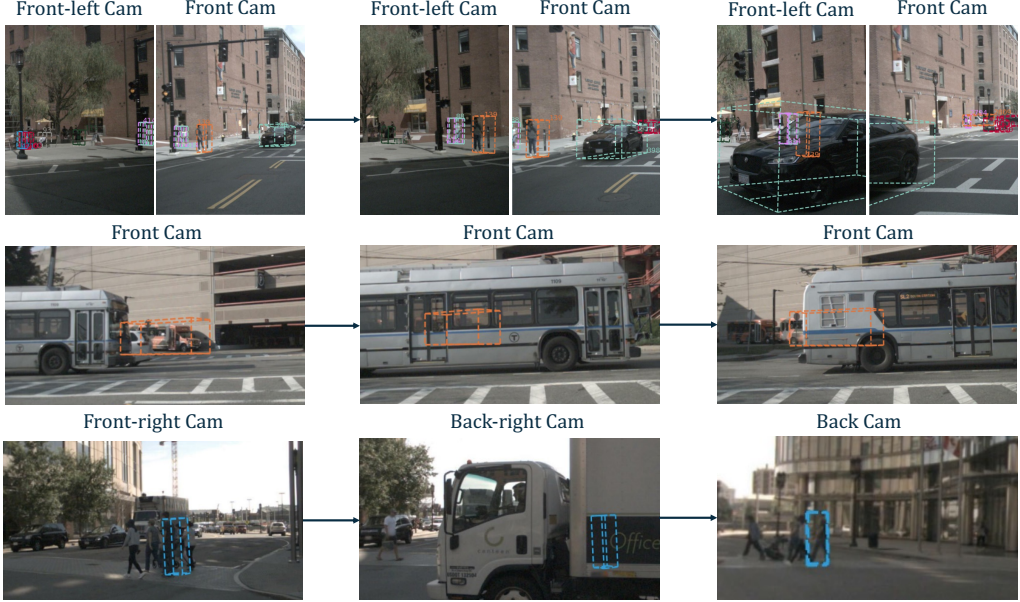


Figure 6. **Qualitative results for 3D MOT.** (1) In the top row, we provide image-level 3D MOT results. The figures highlight the consistency across images, such as the vehicles crossing the front-left and front cameras. (2) In the middle and bottom rows, we provide two dedicated examples for addressing large and small objects’ occlusions.

Method	ADE \downarrow (@4.0s)	FDE \downarrow (@4.0s)
LSTM [7]	2.32	2.87
VectorNet [15]	2.01	2.48
Velocity	2.10	2.64
PF-Track (Ours)	1.88	2.38

Table 5. **Motion prediction from features and abstract states.**

We build a motion prediction benchmark from the true-positive tracks of PF-Track on nuScenes validation split, then train LSTM [7] and VectorNet [15] from the 3D positions of tracks. The “Velocity” row is the result under the assumption of a constant velocity motion model. The results indicate that predicting from features provides richer information for better trajectory quality.

Maps in these experiments. In addition, we report another baseline which uses the velocities predicted by our model’s decoder for trajectory prediction assuming a constant velocity motion model (third row in Tab. 5). The evaluation metrics are “average displacement error” (ADE) and “final displacement error” (FDE), which are better with lower values. More details are in the appendix (Sec. B.5).

Tab. 5 compares the performance between the end-to-end PF-Track and the baselines described above on the validation split of nuScenes. With a lower ADE and FDE, PF-Track has better trajectory quality. Our conclusions agree with previous studies [17, 38, 62]. More specifically, LSTM is a shallow model, unable to capture meaningful dynamics from noisy tracks; the stronger VectorNet can perform better than the other baselines but it is still worse than forecasting trajectories in an end-to-end framework, as proposed in our method.

4.5. Qualitative Results

We visualize the 3D MOT results in Fig. 6 by projecting 3D bounding boxes onto images. The colors of bounding boxes are randomly selected from a pool of seven colors according to their IDs so that each object has a consistent color over time.

In the top row, we provide an overall visualization of multi-camera 3D MOT, focusing on front-left and front cameras. As clearly shown, PF-Track can track objects coherently, especially for the pedestrians and vehicles shown on two separate cameras. In the bottom two rows of Fig. 6, we illustrate two examples of addressing occlusions. For both large (bus) and small (pedestrian) objects, our method propagates their positions during the occluded frames and successfully re-associates them on de-occlusion frames. We highlight that this is achieved without an explicit re-identification module.

5. Conclusions

This paper proposes a query-based end-to-end method for multi-camera 3D MOT that enhances spatio-temporal coherence. By past reasoning, our framework enhances the query features and track quality with historical information. By future reasoning, the predicted trajectories better propagate the queries across adjacent frames and occluded long-term periods. We also demonstrate that joint past and future reasoning further strengthens the tracker’s ability. Extensive evaluation of the large-scale nuScenes dataset demonstrates that our method is effective in providing coherent tracks.

Appendix

Our appendix describes the additional experimental analysis and implementation details. The catalog is as below:

- (A) **Video demo.** We provide a demo for multi-camera 3D multi-object tracking (MOT) as explained in Sec. A.
- (B) **Implementation details.** We explain the detailed model architecture, procedures for training and inference, and settings for ablation studies in Sec. B.
- (C) **Additional ablations.** We provide more analysis and experimental results in Sec. C.
- (D) **Performance Verification.** For checking the results, we provide the screenshot of the test split results for verification in Sec. D.

A. Multi-camera Tracking Video Demo

Our demo video is at <https://youtu.be/eJghONb2AGg>. It contains:

- Visualization of 3D MOT results on both surrounding images and Bird’s-eye-view.
- Illustration for addressing occlusions.
- Qualitative results for predicted trajectories.

B. Implementation Details

B.1. Model Architecture

We explain the design choices of PF-Track in the sections below. To provide a high-level view of the model, we enclose the config file in mmdetection3d [10] format in this supplementary material.

Backbone. We use VoVNetV2 [26] as backbone. For the feature pyramid [30], the C5 feature (output of the 5-th stage) is upsampled and fused with C4 feature (output of the 4-th stage). To save GPU memory during training, we adopt the checkpointing trick [8] by default.

Detection head. We follow the design of PETR [32] by setting the region to $[-51.2m, 51.2m]$ on the XY-axis and $[-5m, 3m]$ on the Z-axis. The centers of bounding boxes are normalized to $[0, 1]$, respectively. The detection head composes of 6 transformer decoder layers [57] and 2 MLP heads for bounding box regression and classification. Each transformer decoder layer has an embedding dimension of 256 and a feedforward dimension of 2048. The dropout probability is 0.1. The MLP heads are both two-layer MLPs. The bounding box regression head predicts the centers (x, y, z) , sizes (l, w, h) , orientation, and velocities of objects, and the classification head returns the logits for every category.

PF-Track configurations. Our PF-Track uses a fixed number of 500 detection queries per frame. As for track queries, the training and inference procedures are differ-

ent. Training protocol adds queries into the set of track queries once they become a positive match to the ground truth ($<2.0m$), and a tracking query is kept associated with the ground truth of the same object. The inference protocol initializes the track queries if the corresponding confidence score is larger than 0.4. During the inference time, our model output at most 300 objects (same as [32, 60, 72]) and set a minimum score threshold of 0.2.

Past reasoning. The length of the query queue is 1.5 seconds ($\tau_h = 3$ frames) because each of our training samples has 3 frames. However, we emphasize that PF-Track is able to aggregate historical information from the entire video during the *inference* time because the past reasoning module is recurrent. Concretely, the queries at frame t attend to frames $[t-2, t]$, and the queries at frame $t-2$, in turn, attend to frames $[t-4, t-2]$, and so on. Thus, the queries at frame t have access to information from all the previous frames.

For cross-frame and cross-frame attention, we employ two transformer decoder layers for them each. Every transformer decoder layer has an embedding dimension of 256, and a feedforward dimension of 2048. Same as the transformer layers in the detection head, these two layers also have a dropout probability of 0.1. The track refinement module uses two separate 2-layer MLP heads for regression and classification.

Future reasoning. The future reasoning module predicts the movements to future 4.0 seconds ($\tau_f = 8$ frames). It first uses the same cross-frame attention to generate the future features, then applies a 2-layer MLP to translate features into the movements on the XY plane. For track extension, we pick the extension length that maximizes the AMOTA on the validation split, which are $2.0s$ (4 frames) for the small resolution model and $2.5s$ (5 frames) for the full resolution model.

Loss weights. In Sec. 3.4 of the main paper, we use coefficients to balance the loss terms. The bounding box regression loss is $\lambda_{box}^D = 0.25$, and the classification focal loss is $\lambda_{cls}^D = 2.0$, which are the same as [32]. For the track refinement part, we adopt the same loss weights for bounding box regression and classification, respectively: $\lambda_{box}^R = 0.25$ and $\lambda_{cls}^R = 2.0$. The weight for motion prediction in future reasoning is $\lambda_f = 0.5$.

B.2. Algorithm for “Track Extension”

We clarify the detailed steps for the track extension algorithms described in Sec. 3.3 (main paper). The pseudo-codes are in Algorithm A.

The track extension algorithm only addresses the low-confidence objects (Line 3). Without track extension, the information of these objects is always updated according

Algorithm A Algorithm for “Track Extension”.

Input:

\mathbf{Q}_{t-1} , \mathbf{C}_{t-1} , $\mathbf{M}_{t:t+\tau_f}^{t-1}$: queries, center positions, and motion predictions from frame $t-1$;
 \mathbf{Q}_t^R , \mathbf{C}_t^R , \mathbf{S}_t^R , $\mathbf{M}_{t+1:t+\tau_f+1}^R$: queries, center positions, confidence scores, and motion predictions decoded from frame t ;
 \mathbf{L}_t : how many frames have the queries been extended continuously;
 τ_e : maximum frames for extension;
 N : number of queries.

Output:

$\mathbf{Prop}(\mathbf{Q}_t)$, $\mathbf{Prop}(\mathbf{C}_t)$, $\mathbf{Prop}(\mathbf{M}_{t+1:t+\tau_f+1}^t)$: propagated queries, bounding boxes, and motion predictions from frame t to frame $t+1$.

```

1: for  $i = 0$  to  $N - 1$  do
2:   if  $S_t^{R,i}$  is below a threshold then
3:     if  $L_t^i < \tau_e$  then
4:        $\mathbf{C}_t^i \leftarrow \mathbf{C}_t^{R,i} + \mathbf{M}_{t:t+1}^{t-1,i}$ 
5:        $\mathbf{Q}_t^i \leftarrow \mathbf{Q}_{t-1}^i$ 
6:        $\mathbf{M}_{t+1:t+\tau_f+1}^t \leftarrow \text{Padding}(\mathbf{M}_{t+1:t+\tau_f}^{t-1})$ 
7:        $L_t^i \leftarrow L_t^i + 1$ 
8:     else
9:       Terminate the track of the  $i$ -th object.
10:      Remove it from memory.
11:    end if
12:  else
13:     $\mathbf{C}_t^i \leftarrow \mathbf{C}_t^{R,i} + \mathbf{M}_{t:t+1}^{t,i}$ 
14:     $\mathbf{Q}_t^i \leftarrow \mathbf{Q}_t^{R,i}$ 
15:     $L_t^i \leftarrow 0$ 
16:  end if
17: end for
18: return  $\mathbf{Q}_t$ ,  $\mathbf{C}_t$ ,  $\mathbf{M}_{t+1:t+\tau_f+1}^t$ 
  
```

to the latest frame (line 13-15). However, track extension relies more on the frames with higher confidence to propagate queries with larger fidelity (Line 4-7). If an object does not have confident results in τ_e continuous frames, we follow the common practice of terminate this track (Line 9-10). Please note that we set τ_e smaller than the prediction horizon $\tau_f = 8$ frames (4.0s) by default. As in Tab. 2, track extension effectively improves both AMOTA and IDS.

B.3. Model Training

Every training sample composes of three adjacent frames. PF-Track is trained with AdamW optimizer [24, 36] with an weight decay of 0.01. The learning rate starts from 2.0×10^{-4} and is scheduled according to cosine annealing [35]. The above process is identical to image-based 3D detection methods [32, 60]. However, as image data aug-

mentation could break the motion models of objects, we disable the data augmentation during the training of the tracker. The total training epochs follow the settings discussed in Sec. 4.2 (main paper). The full resolution setting takes 3 days on $8 \times$ A100 GPUs, and the small resolution setting takes 1 day on $8 \times$ A100 GPUs.

B.4. “Tracking by Detection” Experiments

The experiments of “tracking by detection” baselines in Sec. 4.4 (main paper) tune the detection score threshold according to AMOTA on the validation split. Eventually, we set a minimum score threshold of 0.2 for output bounding boxes, which is also the same as PF-Track. According to Tab. 4 (main paper), our hyper-parameter tuning significantly improves the performance of “tracking by detection” baselines and enables a fair comparison. The reason is that AB3DMOT [63], CenterPoint [68], and SimpleTrack [42] designed their trackers for LiDAR-based 3D detection and used low (e.g., 0.01 in SimpleTrack) or no score thresholds. However, image-based detection contains more false positives and requires stronger filtering.

B.5. Motion Prediction from Abstract Object States Settings

This section explains the details of the “Prediction from Query Features” in Sec. 4.4 (main paper).

Dataset construction. We construct the motion prediction dataset by recalling the true positive tracks from the output of PF-Track. Specifically, we perform Hungarian matching between the predicted bounding boxes and ground truth, and the positive matches are determined by less than 2.0m from the ground truth. We use the training/validation split of nuScenes [3] dataset and remove the frames without positive match. Eventually, we have 27,960 and 5,879 frames, and 422,167 and 69,804 tracks in the training and validation set for motion prediction.

Model training and inference. Our model architectures are the same as the LSTM model from the Argoverse [7] and VectorNet [15]. We provide 2.0s of history and require the model to predict up to 4.0s, which is the same as our PF-Track, for a fair comparison. As every frame contains multiple tracks, our implementation normalizes the coordinates with respect to the positions of ego-vehicle, following [12]. The inputs to the models include the bounding box centers and velocities on the XY plane. For missing observations, we pad the input to the full length with the closest observation and indicate padding with a 0-1 mask. We train the models for 24 epochs on our custom motion prediction dataset with AdamW [24, 36] optimizer and an initial learning rate of 1.0×10^{-3} . The learning rate drops by 0.1 on the 16-th and 20-th epochs.

Model	Extension	AMOTA \uparrow	AMOTP \downarrow	IDS \downarrow
PF-Track	✓	0.391 0.408	1.387 1.343	471 166
wo/ Cross-frame	✓	0.385 0.395	1.402 1.373	410 171
wo/ Cross-object	✓	0.383 0.399	1.390 1.352	481 155

Table A. **Cross-frame and Cross-object attention.** “Extension” denotes using track extension or not. Removing either cross-frame or cross-object from the “Query Refinement” module of past reasoning (Sec. 3.2 of main paper) negatively impacts the model performance.

Model	Extension	AMOTA \uparrow	AMOTP \downarrow	IDS \downarrow
PF-Track	✓	0.391 0.408	1.387 1.343	471 166
Velo Prop	✓	0.374 0.382	1.389 1.359	478 192

Table B. **Velocity for Query Propagation.** “Extension” means using track extension. Using velocities instead of learned trajectories for query propagation in future reasoning (Sec. 3.3 of main paper) negatively impacts the model performance.

C. Supplemental Ablation Studies

C.1. Cross-frame and Cross-object Attention in Past Reasoning.

We analyze the effect of cross-frame and cross-object attention for “Query Refinement” in past reasoning (Sec. 3.2 of main paper). As in Tab. A, if either of them is removed from the final PF-Track, the performance decreases, especially in AMOTA. Although PF-Track has a slightly larger ID-Switch, we argue that it is due to a higher AMOTA. Therefore, both cross-frame and cross-object attentions are useful for multi-camera 3D MOT.

C.2. Trajectories or Velocity for Query Propagation

To verify the necessity of learning a trajectory prediction for query propagation, we experiment with using the velocities for propagation in Tab. B. Specifically, we train a model identical to PF-Track except using velocities to transform the positions of queries across frames. As in Tab. B, using learned trajectories has a better performance compared with the variant of using velocities. Therefore, we conclude that learning long-term trajectory prediction is necessary for robust and accurate 3D MOT.

C.3. Weights of Motion Prediction in Future Reasoning

We analyze the tracking performance with respect to the loss weights of motion prediction. The discovery is the sensitivity of tracking performance to the weight of the loss for motion prediction λ_f (Sec. 3.4 in main paper). In Tab. C, we vary the weight for motion prediction with

λ_f	Extension	AMOTA \uparrow	AMOTP \downarrow	IDS \downarrow
0.25	✓	0.389 0.396	1.382 1.353	539 185
0.50	✓	0.391 0.408	1.387 1.343	471 166
1.00	✓	0.377 0.397	1.395 1.346	489 183

Table C. **Loss weights of motion prediction.** “ λ_f ” denotes the loss weight λ_f for motion prediction (Sec. 3.4 in main paper), “Extension” denotes using track extension or not. This table demonstrates the sensitivity of motion prediction and calls for the attention of future work in better multi-task learning strategies.

Validation Set Bounding Box Number

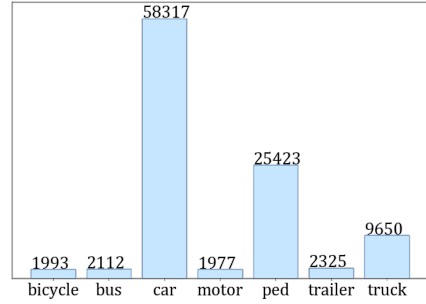


Figure A. Distribution of per-category instance numbers in nuScenes validation set. “motor” denotes “motorcycle” and “ped” denotes “pedestrian.” As clearly demonstrated, the data distribution is imbalanced on nuScenes.

$\lambda_f = [0.25, 0.50, 1.00]$, and they could cause variation in the tracking performance. This requires the attention of future works or better multi-task learning strategies

C.4. Category-level Analysis

We compare the category-level performance before and after using our past and future reasoning. To provide the context of nuScenes dataset [3], we start by visualizing the data distribution across categories in Fig. A. As clearly illustrated, nuScenes exhibits an imbalanced category distribution, and the types of “car” and “pedestrian” take up most of the objects.

Then in Tab. D, we compare the category-level performance of the three major types: car, pedestrian, and truck. Compared to the baseline of not using any past or future reasoning (same baseline as Tab. 2 of the main paper), our proposed method significantly improves upon the baseline over individual categories.

C.5. PF-Track with DETR3D

We provide supplemental analysis of applying PF-Track to a different 3D detector: DETR3D [60].

Experiment setup. Following DETR3D [60], we use VoVNetV2 [26] as the backbone and fuse the features from C2-C5 with FPN [30] as the image features. As DETR3D

```

Calculating metrics...
Saving metrics to: /tmp/tmp_bimu3cd/nuscenes-metrics

## Final results ##

Per-class results:
  AMOTA  AMOTP  RECALL  MOTAR  GT    MOTA  MOTP  MT    ML    FAF  TP    FP    FN    IDS  FRAG  TID  LGD
bicycle  0.322  1.442  0.387  0.762  2186  0.295  0.635  46   102   14.7  845  201  1341  0    8    1.48  1.87
bus      0.408  1.257  0.544  0.605  1701  0.329  0.720  36   33    25.3  924  365  776  1    21   1.92  2.48
car      0.622  0.916  0.719  0.777  68518  0.558  0.520  2443  1371  186.6  49194  10956  19225  99   415   0.87  1.19
motorcy  0.448  1.245  0.457  0.840  1945  0.384  0.561  41   87    11.5  888  142  1057  0    5    1.31  1.61
pedestr  0.451  1.279  0.541  0.736  34010  0.395  0.738  734  873   96.9  18250  4827  15618  142   273  1.52  2.16
trailer  0.380  1.421  0.528  0.636  2566  0.334  0.884  57   64    48.7  1350  492  1212  4    23   0.99  1.61
truck    0.405  1.206  0.592  0.596  8639  0.352  0.658  191  178   51.1  5107  2065  3529  3    94   1.11  2.07

Aggregated results:
AMOTA  0.434
AMOTP  1.252
RECALL 0.538
MOTAR  0.707
GT     17080
MOTA   0.378
MOTP   0.674
MT     3548
ML     2708
FAF    62.1
TP     76558
FP     19048
FN     42758
IDS    249
FRAG   839
TID    1.32
LGD    1.86
Eval time: 5146.9s

Completed evaluation for test phase

```

Figure B. **Screenshot of test set result.** This is in supplementary for our results in Tab. 1 (main paper).

Metrics	PF-Track	Car	Pedestrian	Truck	All
AMOTA \uparrow	✓	0.562 0.579	0.372 0.415	0.374 0.403	0.358 0.408
AMOTP \downarrow	✓	1.058 1.021	1.431 1.362	1.341 1.288	1.419 1.343
IDS \downarrow	✓	368 67	154 83	25 7	507 166

Table D. **Per-category tracking metrics analysis.** “All” denotes the averaged metric numbers over all seven categories. On the three major categories on nuScenes, our PF-Track achieves significant and steady improvement over the baseline that does not involve past or future reasoning.

Metrics	PF-Track	Car	Pedestrian	Truck	All
AMOTA \uparrow	✓	0.583 0.600	0.370 0.431	0.305 0.310	0.344 0.362
AMOTP \downarrow	✓	1.038 1.001	1.436 1.338	1.399 1.366	1.419 1.363
IDS \downarrow	✓	394 172	222 116	32 5	680 300

Table E. **PF-Track for DETR3D detection head.** “All” denotes the averaged metric numbers over all seven categories, “PF-Track” denotes using the past and future reasoning from PF-Track. On the three major categories and average metrics on nuScenes, PF-Track is able to enhance the tracking performance.

only has a full-resolution setting, we first train the backbone with single-frame detection for 24 Epochs, then fix the backbone and train the whole tracker with 3-frame tracking for another 24 Epochs. A cycle of training takes 3 days on $8 \times$ A100 GPUs.

Efficacy of PF-Track. We analyze the performance without or with the joint past and future reasoning in PF-Track in Tab. E. We include the results for top-3 major categories and the average of all categories. Our past and future reasoning also significantly improves the AMOTA and decreases ID-Switches. This result indicates the generalizability of PF-Track on other query-based detectors.

D. Test Split Screenshot

We provide the screenshot of the submission to nuScenes test set in Fig. B, as supplementary to the test set results in Tab. 1 (main paper).

References

- [1] Keni Bernardin and Rainer Stiefelhagen. Evaluating multiple object tracking performance: the clear MOT metrics. *EURASIP Journal on Image and Video Processing*, 2008. 6
- [2] Alex Bewley, Zongyuan Ge, Lionel Ott, Fabio Ramos, and Ben Upcroft. Simple online and realtime tracking. In *ICIP*, 2016. 2
- [3] Holger Caesar, Varun Bankiti, Alex H Lang, Sourabh Vora, Venice Erin Liou, Qiang Xu, Anush Krishnan, Yu Pan, Giacomo Baldan, and Oscar Beijbom. nuScenes: A multimodal dataset for autonomous driving. In *CVPR*, 2020. 1, 2, 6, 10, 11
- [4] Nicolas Carion, Francisco Massa, Gabriel Synnaeve, Nicolas Usunier, Alexander Kirillov, and Sergey Zagoruyko. End-to-end object detection with transformers. In *ECCV*, 2020. 2, 3

[5] Sergio Casas, Abbas Sadat, and Raquel Urtasun. MP3: A unified model to map, perceive, predict and plan. In *CVPR*, 2021. 3

[6] Mohamed Chaabane, Peter Zhang, J Ross Beveridge, and Stephen O’Hara. DEFT: Detection embeddings for tracking. *arXiv preprint arXiv:2102.02267*, 2021. 1, 6

[7] Ming-Fang Chang, John Lambert, Patsorn Sangkloy, Jagjeet Singh, Slawomir Bak, Andrew Hartnett, De Wang, Peter Carr, Simon Lucey, Deva Ramanan, et al. Argoverse: 3D tracking and forecasting with rich maps. In *CVPR*, 2019. 1, 3, 7, 8, 10

[8] Tianqi Chen, Bing Xu, Chiyuan Zhang, and Carlos Guestrin. Training deep nets with sublinear memory cost. *arXiv preprint arXiv:1604.06174*, 2016. 9

[9] Hsu-kuang Chiu, Jie Li, Rareş Ambruş, and Jeannette Bohg. Probabilistic 3D multi-modal, multi-object tracking for autonomous driving. In *ICRA*, 2021. 2

[10] MMDetection3D Contributors. MMDetection3D: Open-MMLab next-generation platform for general 3D object detection. <https://github.com/open-mmlab/mmdetection3d>, 2020. 9

[11] Patrick Dendorfer, Vladimir Yugay, Aljoša Ošep, and Laura Leal-Taixé. Quo Vadis: Is trajectory forecasting the key towards long-term multi-object tracking? In *NeurIPS*, 2022. 3

[12] Scott Ettinger, Shuyang Cheng, Benjamin Caine, Chenxi Liu, Hang Zhao, Sabeek Pradhan, Yuning Chai, Ben Sapp, Charles R Qi, Yin Zhou, et al. Large scale interactive motion forecasting for autonomous driving: The waymo open motion dataset. In *ICCV*, 2021. 1, 3, 10

[13] Tobias Fischer, Yung-Hsu Yang, Suryansh Kumar, Min Sun, and Fisher Yu. CC-3DT: Panoramic 3D object tracking via cross-camera fusion. In *CoRL*, 2022. 1, 2, 6

[14] Huan Fu, Mingming Gong, Chaohui Wang, Kayhan Batmanghelich, and Dacheng Tao. Deep ordinal regression network for monocular depth estimation. In *CVPR*, 2018. 2

[15] Jiyang Gao, Chen Sun, Hang Zhao, Yi Shen, Dragomir Anguelov, Congcong Li, and Cordelia Schmid. VectorNet: Encoding HD maps and agent dynamics from vectorized representation. In *CVPR*, 2020. 3, 4, 7, 8, 10

[16] Clément Godard, Oisin Mac Aodha, Michael Firman, and Gabriel J Brostow. Digging into self-supervised monocular depth estimation. In *ICCV*, 2019. 2

[17] Junru Gu, Chenxu Hu, Tianyuan Zhang, Xuanyao Chen, Yilun Wang, Yue Wang, and Hang Zhao. ViP3D: End-to-end visual trajectory prediction via 3D agent queries. *arXiv preprint arXiv:2208.01582*, 2022. 1, 8

[18] Vitor Guizilini, Rares Ambrus, Sudeep Pillai, Allan Raventos, and Adrien Gaidon. 3D packing for self-supervised monocular depth estimation. In *CVPR*, 2020. 2

[19] Anthony Hu, Zak Murez, Nikhil Mohan, Sofía Dudas, Jeffrey Hawke, Vijay Badrinarayanan, Roberto Cipolla, and Alex Kendall. FIERY: Future instance prediction in bird’s-eye view from surround monocular cameras. In *ICCV*, 2021. 3

[20] Hou-Ning Hu, Yung-Hsu Yang, Tobias Fischer, Trevor Darrell, Fisher Yu, and Min Sun. Monocular quasi-dense 3D object tracking. *IEEE Transactions on Pattern Analysis and Machine Intelligence*, 2022. 1, 2, 6

[21] Junjie Huang, Guan Huang, Zheng Zhu, and Dalong Du. BEVDet: High-performance multi-camera 3D object detection in bird-eye-view. *arXiv preprint arXiv:2112.11790*, 2021. 1, 2

[22] Boris Ivanovic, Kuan-Hui Lee, Pavel Tokmakov, Blake Wulfe, Rowan McAllister, Adrien Gaidon, and Marco Pavone. Heterogeneous-agent trajectory forecasting incorporating class uncertainty. *arXiv preprint arXiv:2104.12446*, 2021. 1

[23] Boris Ivanovic and Marco Pavone. The trajectron: Probabilistic multi-agent trajectory modeling with dynamic spatiotemporal graphs. In *ICCV*, 2019. 3

[24] Diederik P Kingma and Jimmy Ba. Adam: A method for stochastic optimization. *arXiv preprint arXiv:1412.6980*, 2014. 10

[25] Alex H Lang, Sourabh Vora, Holger Caesar, Lubing Zhou, Jiong Yang, and Oscar Beijbom. PointPillars: Fast encoders for object detection from point clouds. In *CVPR*, 2019. 2

[26] Youngwan Lee, Joong-won Hwang, Sangrok Lee, Yuseok Bae, and Jongyoul Park. An energy and gpu-computation efficient backbone network for real-time object detection. In *CVPRW*, 2019. 9, 11

[27] Yinhao Li, Zheng Ge, Guanyi Yu, Jinrong Yang, Zengran Wang, Yukang Shi, Jianjian Sun, and Zeming Li. BEVDepth: Acquisition of reliable depth for multi-view 3d object detection. *arXiv preprint arXiv:2206.10092*, 2022. 1, 2

[28] Zhiqi Li, Wenhui Wang, Hongyang Li, Enze Xie, Chong-hao Sima, Tong Lu, Qiao Yu, and Jifeng Dai. BEVFormer: Learning bird’s-eye-view representation from multi-camera images via spatiotemporal transformers. In *ECCV*, 2022. 1, 2

[29] Ming Liang, Bin Yang, Wenyuan Zeng, Yun Chen, Rui Hu, Sergio Casas, and Raquel Urtasun. PnPNet: End-to-end perception and prediction with tracking in the loop. In *CVPR*, 2020. 3

[30] Tsung-Yi Lin, Piotr Dollár, Ross Girshick, Kaiming He, Bharath Hariharan, and Serge Belongie. Feature pyramid networks for object detection. In *CVPR*, 2017. 9, 11

[31] Tsung-Yi Lin, Priya Goyal, Ross Girshick, Kaiming He, and Piotr Dollár. Focal loss for dense object detection. In *ICCV*, 2017. 5

[32] Yingfei Liu, Tiancai Wang, Xiangyu Zhang, and Jian Sun. PETR: Position embedding transformation for multi-view 3D object detection. In *ECCV*, 2022. 1, 2, 4, 6, 7, 9, 10

[33] Yingfei Liu, Junjie Yan, Fan Jia, Shuaolin Li, Qi Gao, Tiancai Wang, Xiangyu Zhang, and Jian Sun. PETRv2: A unified framework for 3D perception from multi-camera images. *arXiv preprint arXiv:2206.01256*, 2022. 2

[34] Yicheng Liu, Jinghuai Zhang, Liangji Fang, Qinrong Jiang, and Bolei Zhou. Multimodal motion prediction with stacked transformers. In *CVPR*, 2021. 3

[35] Ilya Loshchilov and Frank Hutter. SGDR: Stochastic gradient descent with warm restarts. *arXiv preprint arXiv:1608.03983*, 2016. 10

[36] Ilya Loshchilov and Frank Hutter. Decoupled weight decay regularization. *arXiv preprint arXiv:1711.05101*, 2017. 10

[37] Jonathon Luiten, Tobias Fischer, and Bastian Leibe. Track to reconstruct and reconstruct to track. *Robotics and Automation Letters*, 2020. 1, 2

[38] Wenjie Luo, Bin Yang, and Raquel Urtasun. Fast and furious: Real time end-to-end 3D detection, tracking and motion forecasting with a single convolutional net. In *CVPR*, 2018. 3, 7, 8

[39] Nicola Marinello, Marc Proesmans, and Luc Van Gool. TripletTrack: 3D object tracking using triplet embeddings and lstm. In *CVPR*, 2022. 1, 6

[40] Tim Meinhardt, Alexander Kirillov, Laura Leal-Taixe, and Christoph Feichtenhofer. TrackFormer: Multi-object tracking with transformers. In *CVPR*, 2022. 2, 3

[41] Jiquan Ngiam, Benjamin Caine, Vijay Vasudevan, Zhengdong Zhang, Hao-Tien Lewis Chiang, Jeffrey Ling, Rebecca Roelofs, Alex Bewley, Chenxi Liu, Ashish Venugopal, et al. Scene transformer: A unified multi-task model for behavior prediction and planning. In *ICLR*, 2021. 3, 4, 5

[42] Ziqi Pang, Zhichao Li, and Naiyan Wang. Simpletrack: Understanding and rethinking 3D multi-object tracking. *arXiv preprint arXiv:2111.09621*, 2021. 1, 2, 5, 7, 10

[43] Dennis Park, Rares Ambrus, Vitor Guizilini, Jie Li, and Adrien Gaidon. Is pseudo-LiDAR needed for monocular 3D object detection? In *ICCV*, 2021. 2

[44] C Peng, W Jiang, Y Quanzeng, L Haibin, and L Zicheng. TransMOT: Spatial-temporal graph transformer for multiple object tracking. In *CVPR*, 2021. 2

[45] Neehar Peri, Jonathon Luiten, Mengtian Li, Aljoša Ošep, and Laura Leal-Taixé. Forecasting from LiDAR via future object detection. In *CVPR*, 2022. 3

[46] John Phillips, Julieta Martinez, Ioan Andrei Bârsan, Sergio Casas, Abbas Sadat, and Raquel Urtasun. Deep multi-task learning for joint localization, perception, and prediction. In *CVPR*, 2021. 3

[47] Cody Reading, Ali Harakeh, Julia Chae, and Steven L. Waslander. Categorical depth distribution network for monocular 3D object detection. *CVPR*, 2021. 2

[48] Tim Salzmann, Boris Ivanovic, Punarjay Chakravarty, and Marco Pavone. Trajectron++: Dynamically-feasible trajectory forecasting with heterogeneous data. In *ECCV*, 2020. 3

[49] Samuel Scheidegger, Joachim Benjaminsson, Emil Rosenberg, Amrit Krishnan, and Karl Granström. Mono-camera 3D multi-object tracking using deep learning detections and pmbm filtering. In *IV*, 2018. 1, 2

[50] Meet Shah, Zhiling Huang, Ankit Laddha, Matthew Langford, Blake Barber, Sidney Zhang, Carlos Vallespi-Gonzalez, and Raquel Urtasun. LiRaNet: End-to-end trajectory prediction using spatio-temporal radar fusion. *arXiv preprint arXiv:2010.00731*, 2020. 3

[51] Shaoshuai Shi, Li Jiang, Dengxin Dai, and Bernt Schiele. Motion transformer with global intention localization and local movement refinement. In *NeurIPS*, 2022. 3

[52] Colton Stearns, Davis Rempe, Jie Li, Rares Ambrus, Sergey Zakharov, Vitor Guizilini, Yanchao Yang, and Leonidas J Guibas. SpOT: Spatiotemporal modeling for 3D object tracking. In *ECCV*, 2022. 2

[53] Peize Sun, Jinkun Cao, Yi Jiang, Rufeng Zhang, Enze Xie, Zehuan Yuan, Changhu Wang, and Ping Luo. TransTrack: Multiple object tracking with transformer. *arXiv preprint arXiv:2012.15460*, 2020. 2

[54] Pei Sun, Henrik Kretzschmar, Xerxes Dotiwalla, Aurelien Chouard, Vijaysai Patnaik, Paul Tsui, James Guo, Yin Zhou, Yuning Chai, Benjamin Caine, et al. Scalability in perception for autonomous driving: Waymo open dataset. In *CVPR*, 2020. 3

[55] Siyu Tang, Mykhaylo Andriluka, Bjoern Andres, and Bernt Schiele. Multiple people tracking by lifted multicut and person re-identification. In *CVPR*, 2017. 2

[56] Pavel Tokmakov, Jie Li, Wolfram Burgard, and Adrien Gaidon. Learning to track with object permanence. In *ICCV*, 2021. 2, 6

[57] Ashish Vaswani, Noam Shazeer, Niki Parmar, Jakob Uszkoreit, Llion Jones, Aidan N Gomez, Łukasz Kaiser, and Illia Polosukhin. Attention is all you need. *NeurIPS*, 2017. 9

[58] Qitai Wang, Yuntao Chen, Ziqi Pang, Naiyan Wang, and Zhaoxiang Zhang. Immortal tracker: Tracklet never dies. *arXiv preprint arXiv:2111.13672*, 2021. 2

[59] Tai Wang, Xinge Zhu, Jiangmiao Pang, and Dahua Lin. FCOS3D: Fully convolutional one-stage monocular 3D object detection. In *ICCV*, 2021. 2

[60] Yue Wang, Vitor Campagnolo Guizilini, Tianyuan Zhang, Yilun Wang, Hang Zhao, and Justin Solomon. DETR3D: 3D object detection from multi-view images via 3D-to-2D queries. In *CoRL*, 2022. 1, 2, 9, 10, 11

[61] Xinshuo Weng, Boris Ivanovic, Kris Kitani, and Marco Pavone. Whose track is it anyway? Improving robustness to tracking errors with affinity-based trajectory prediction. In *CVPR*, 2022. 3

[62] Xinshuo Weng, Boris Ivanovic, and Marco Pavone. MTP: Multi-hypothesis tracking and prediction for reduced error propagation. In *IV*, 2022. 3, 8

[63] Xinshuo Weng, Jianren Wang, David Held, and Kris Kitani. 3D multi-object tracking: A baseline and new evaluation metrics. In *IROS*, 2020. 2, 6, 7, 10

[64] Xinshuo Weng, Jianren Wang, Sergey Levine, Kris Kitani, and Nicholas Rhinehart. Inverting the pose forecasting pipeline with SPF2: Sequential pointcloud forecasting for sequential pose forecasting. In *CoRL*, 2021. 3

[65] Xinshuo Weng, Yongxin Wang, Yunze Man, and Kris M Kitani. GNN3DMOT: Graph neural network for 3D multi-object tracking with 2D-3D multi-feature learning. In *CVPR*, 2020. 1, 2

[66] Benjamin Wilson, William Qi, Tanmay Agarwal, John Lambert, Jagjeet Singh, Siddhesh Khandelwal, Bowen Pan, Ratnesh Kumar, Andrew Hartnett, Jhony Kaesemel Pontes, et al. Argoverse 2: Next generation datasets for self-driving perception and forecasting. In *NeurIPS*, 2022. 1, 3

[67] Nicolai Wojke, Alex Bewley, and Dietrich Paulus. Simple online and realtime tracking with a deep association metric. In *ICIP*, 2017. 2

[68] Tianwei Yin, Xingyi Zhou, and Philipp Krahenbuhl. Center-based 3D object detection and tracking. In *CVPR*, 2021. 2, 7, 10

- [69] Ye Yuan, Xinshuo Weng, Yanglan Ou, and Kris M Kitani. AgentFormer: Agent-aware transformers for socio-temporal multi-agent forecasting. In *ICCV*, 2021. [3](#)
- [70] Jan-Nico Zaech, Alexander Liniger, Dengxin Dai, Martin Danelljan, and Luc Van Gool. Learnable online graph representations for 3D multi-object tracking. *Robotics and Automation Letters*, 2022. [1](#), [2](#)
- [71] Fangao Zeng, Bin Dong, Tiancai Wang, Xiangyu Zhang, and Yichen Wei. MOTR: End-to-end multiple-object tracking with transformer. In *ECCV*, 2022. [2](#), [3](#)
- [72] Tianyuan Zhang, Xuanyao Chen, Yue Wang, Yilun Wang, and Hang Zhao. MUTR3D: A multi-camera tracking framework via 3D-to-2D queries. In *CVPRW*, 2022. [1](#), [2](#), [3](#), [6](#), [9](#)
- [73] Yifu Zhang, Chunyu Wang, Xinggang Wang, Wenjun Zeng, and Wenyu Liu. FairMOT: On the fairness of detection and re-identification in multiple object tracking. *International Journal of Computer Vision*, 2021. [2](#)
- [74] Yunpeng Zhang, Zheng Zhu, Wenzhao Zheng, Junjie Huang, Guan Huang, Jie Zhou, and Jiwen Lu. BEVerse: Unified perception and prediction in birds-eye-view for vision-centric autonomous driving. *arXiv preprint arXiv:2205.09743*, 2022. [3](#)
- [75] Xingyi Zhou, Vladlen Koltun, and Philipp Krähenbühl. Tracking objects as points. In *ECCV*, 2020. [2](#), [6](#)
- [76] Xizhou Zhu, Weijie Su, Lewei Lu, Bin Li, Xiaogang Wang, and Jifeng Dai. Deformable DETR: Deformable transformers for end-to-end object detection. In *ICLR*, 2021. [3](#)